

# Silencing of a *BYPASS1* homolog results in root-independent pleiotrophic developmental defects in *Nicotiana benthamiana*

Yong Won Kang · Ryong Nam Kim · Hye Sun Cho ·  
Woo Taek Kim · Doil Choi · Hyun-Sook Pai

Received: 25 January 2008 / Accepted: 16 July 2008 / Published online: 21 August 2008  
© Springer Science+Business Media B.V. 2008

**Abstract** The *Arabidopsis bypass1* mutant (*bps1*) exhibits defective shoot and root growth that is associated with constitutive production of a root-derived carotenoid-related signal (Van Norman et al., *Curr Biol* 14:1739–1746, 2004). Since the identity of the signal and the function of BPS1 are still unknown, we investigated effects of BPS1 depletion in *Nicotiana benthamiana* to elucidate BPS1 function in plant growth and development. The predicted protein of *NbBPS1*, a *BPS1* homolog of *N. benthamiana*, contains a central transmembrane domain, and a NbBPS1:GFP fusion protein was mainly associated with the endoplasmic reticulum. Virus-induced gene silencing (VIGS) of *NbBPS1* resulted in pleiotrophic phenotypes, including growth retardation and abnormal leaf development. At the cellular level, the plants exhibited hyperproliferation of the cambial cells and defective xylem differentiation during stem vascular

development. Hyperactivity of the cambium was associated with an elevated auxin and cytokinin response. In contrast, the leaves had reduced numbers of cells with increased cell size and elevated endoreduplication. Cell death in *NbBPS1* VIGS leaves started with vacuole collapse, followed by degeneration of the organelles. Interestingly, these phenotypes were mainly caused by silencing of *NbBPS1* in the aerial parts of the plants, different from the case of the *Arabidopsis bps1* mutant. These results suggest that NbBPS1 plays a role in the control of cell division and differentiation in the cambium of *N. benthamiana*, and *BPS* homologs may have a diverse function in different tissues and in different species.

**Keywords** Cell death · Endoreduplication · ER targeting · Hyperproliferation · Promoter-GUS fusion · Virus-induced gene silencing

Y. W. Kang and R. N. Kim contributed equally to this work.  
GenBank accession numbers: EU243336 (NbBPS1) and EU243335 (NbBPS2).

**Electronic supplementary material** The online version of this article (doi:10.1007/s11103-008-9384-7) contains supplementary material, which is available to authorized users.

Y. W. Kang · W. T. Kim · H.-S. Pai (✉)  
Department of Biology, Yonsei University, Seoul 120-749,  
Korea  
e-mail: hspai@yonsei.ac.kr

R. N. Kim · H. S. Cho  
Plant Genome Research Center, Korea Research Institute of  
Bioscience and Biotechnology, Taejeon 305-333, Korea

D. Choi (✉)  
Department of Plant Sciences, Seoul National University, Seoul  
151-742, Korea  
e-mail: doil@snu.ac.kr

## Introduction

The mechanisms by which cell division is integrated into differentiation and development in the meristems and lateral organ primordia of plants represent a major challenge to plant biologists. Recent studies indicate that developmental signals influence meristem size by controlling the rate of cell division, and that cell cycle components influence meristem patterning and maintenance (Gutierrez 2005; Ramirez-Parra et al. 2005). Phytohormones have long been known to act as long-range signals that integrate developmental, genetic, and environmental information to regulate cell division and differentiation. In particular, auxins and cytokinins directly influence the cell cycle regulators, while other hormones such as brassinosteroids and abscisic acids also affect cell cycle progression

(Dewitte and Murray 2003; Ramirez-Parra et al. 2005; Gegas and Doonan 2006; Cho et al. 2007).

Recent studies provide evidence for a novel class of graft-transmissible molecules through which roots influence shoot branching and leaf development (Booker et al. 2004; Van Norman et al. 2004). The Ramosus (*rms*) mutants of pea and the More Axillary Branching (*max*) mutants of *Arabidopsis* show increased shoot branching, and the bushy shoot phenotype is reversed by grafting mutant shoots to a wild-type rootstock (Foo et al. 2001; Stirnberg et al. 2002; Sorefan et al. 2003) indicating that these genes are required for production of a long-range graft-transmissible signal that inhibits branching. The *MAX4* and *RMS1* genes encode proteins that are homologous to carotenoid cleavage dioxygenases (CCDs), suggesting that the MAX- and RMS-dependent inhibitor of branching is a carotenoid-derived molecule (Sorefan et al. 2003).

The *Arabidopsis bypass1* (*bps1*) mutant, a recessive mutant with shoot and root defects, was originally identified in a screen for leaf vein pattern defects (Van Norman et al. 2004). The *bps1* mutant phenotype is temperature-dependent, being more severe at lower temperature. The BPS1-dependent signal is graft-transmissible, and furthermore, the *bps1* phenotype is partially rescued by supplementation with fluridone, an inhibitor of the carotenoid biosynthetic enzyme phytoene desaturase, whereas none of the classical plant hormones can correct the mutant phenotype (Van Norman et al. 2004). Based on these results, the authors proposed that BPS1 function is required to prevent constitutive production of a carotenoid-related root-derived signal that inhibits shoot development. The *BPS1* gene encodes a protein with no homology to any functionally characterized proteins. The mobile signal is neither ABA nor the MAX-dependent hormone, and requires synthesis of  $\beta$ -carotene and its derivatives, but its identity remains unknown (Van Norman and Sieburth 2007).

In this study, we investigated the cellular function of BPS1 in *N. benthamiana* by virus-induced gene silencing (VIGS). VIGS of *NbBPS1*, a *BPS1* homolog of *N. benthamiana*, resulted in arrested growth and abnormal plant development, correlated with altered activity of the cambium. The uncontrolled proliferation of the cambial cells was associated with an elevated auxin/cytokinin response. The effects of NbBPS1 deficiency on the target tissues of *N. benthamiana* are discussed in relation to the mobile carotenoid-derived signal.

## Materials and methods

### Virus-induced gene silencing

*Nicotiana benthamiana* plants were cultivated in a growth room (24°C) under a regime of 16 h light and 8 h dark.

*NbBPS1* cDNA fragments were PCR-amplified and cloned into the pTV00 vector containing part of the TRV2 genome using BamHI/ApaI sites (Ratcliff et al. 2001). As a control for VIGS, a green fluorescent protein (GFP) cDNA sequence was also cloned into the pTV00 vector. VIGS was performed as described previously (Park et al. 2005; Kim et al. 2006).

### Semiquantitative Reverse Transcription (RT)-PCR

Semiquantitative RT-PCR was performed with 10  $\mu$ g total RNA isolated from the fourth leaf above the infiltrated leaf as described (Kim et al. 2006). To detect endogenous *NbBPS1* and *NbBPS2* transcripts, we used the following primer sets: BPS1-UTR, (5'-caacaatgtacacaaacaatgg-3' and 5'-atactcgaggtataaattgatctgtcagc-3'); BPS1-C2, (5'-ggccccgttcacgagactgtctt-3' and 5'-atactcgaggtataaattgatctgtcagc-3'); BPS1-N, (5'-gggccctcccacaggaaccacacc-3' and 5'-ggatcctccgtccaatgaagaacg-3'); BPS1-C1, (5'-gggccccgc aatgatggagtggagg-3' and 5'-atactcgaggtataaattgatctgtcagc-3'); BPS2-C, (5'-gggccccaagcatttggatcttcgcga-3' and 5'-atactcgaggtataaattgatctgtcagc-3'); BPS2-UTR, (5'-atag aattcgtcttaacctagcacaagcg-3' and 5'-atactcgaggtataaattgatctgtcagc-3').

### Subcellular localization of NbBPS1

A *NbBPS1* cDNA fragment corresponding to the full-length protein was cloned into the 326-GFP plasmid (Lee et al. 2001) using BamHI sites to generate the NbBPS1:GFP fusion protein. The NbBPS1:GFP and the BiP:RFP fusion constructs were introduced into *N. benthamiana* protoplasts by PEG-mediated transformation, and their expression was monitored 24 h after transformation by fluorescent microscopy. Similarly, bZIP28:GFP (Liu et al. 2007) was transformed to *N. benthamiana* protoplasts to show its expression pattern in the ER. GFP and RFP vectors were cotransformed into *N. benthamiana* protoplasts and the fluorescent signal was observed by confocal laser scanning microscopy as described (Cho et al. 2004).

### Histochemical analyses

Transmission electron microscopy, scanning electron microscopy, tissue sectioning, and light microscopy were carried out as described by Ahn et al. (2004) using the fourth or fifth leaf above the infiltrated leaf of the VIGS lines.

### Flow cytometry

Suspensions of nuclei were obtained by chopping leaves and stems of the VIGS plants with a sharp razor blade in nuclei-stabilizing buffer (100 mM TRIS, 50 mM NaCl, 0.1% Triton X-100, pH 7). Propidium iodide (Sigma Chemical

Co.) and DNase-free RNase (Boehringer Mannheim) at final concentrations of 50  $\mu\text{g ml}^{-1}$  and 25  $\mu\text{g ml}^{-1}$ , respectively, were added to the nuclei suspension 30 min before analysis. Nuclear DNA content was measured using FACS-scan flow cytometer (FACSCalibur, Becton-Dickinson) and CellQuest S/W program (version 3.1).

#### Measurement of mitochondrial membrane potential

TMRM (*Tetramethylrhodamine methyl ester*; Molecular Probes) was added to the protoplasts isolated from the fourth leaf above the infiltrated leaf of the VIGS lines to the final concentration of 200 nM. After incubation for 1–2 min at 25°C, the protoplasts were transferred to microscope slide wells and observed with a confocal microscope (Carl Zeiss LSM 510) with optical filters (543 nm excitation, 585 nm emission) to visualize the red fluorescent probe. Quantitative images were captured and data were analyzed using the LSM 510 software (version 2.8).

#### Localization of lignin

Leaf samples were incubated in a phloroglucinol-HCl solution for 2 min at room temperature and pressed gently between a slide and a coverslip for observation.

## Results

### Phylogenetic analysis of BPS1 homologs

The full-length *NbBPS1* cDNA encodes a polypeptide of 352 amino acids with a predicted molecular mass of 39348.75 Da (Fig. 1a). The *N. benthamiana* EST database contains a close homolog of *NbBPS1*, designated *NbBPS2*. *NbBPS1* exhibits 83% nucleotide and 86% amino acid sequence identity to *NbBPS2* in the coding region, but no sequence homology in the 3'-untranslated region (3'-UTR). The *NbBPS1* protein sequence was aligned with *NbBPS2*, Arabidopsis BPS1, At4g01360 and At2g46080, and the related sequences from tomato and rice (Fig. 1a). The alignment indicates that this group of proteins is evolutionarily conserved, although the rice homolog is longer due to additional sequences in the middle and at the C-terminus. The predicted *NbBPS1* and *NbBPS2* proteins as well as the tomato and rice homologs have a single transmembrane domain (residues 195–217 in *NbBPS1*) based on TMHMM (<http://www.cbs.dtu.dk/services/TMHMM/>) (Fig. 1e) and PSORT (<http://psort.hgc.jp/>) programs, indicating membrane association of the proteins. Interestingly, none of the Arabidopsis *BYPASS* genes (*BPS1*, At4g01360 and At2g46080) showed strong probability for the transmembrane domain. The phylogenetic tree of *NbBPS1*

based on Molecular Evolutionary Genetics Analysis (MEGA) (<http://www.megasoftware.net/>) (Tamura et al. 2007) indicates that *NbBPS1* and *NbBPS2* are grouped with the tomato and rice BPS homologs (Fig. 1b).

### Expression of *NbBPS1* and *NbBPS2*

The tissue-specific expression pattern of *NbBPS1* and *NbBPS2* was investigated by semiquantitative RT-PCR using *NbBPS1*- and *NbBPS2*-specific primers (Fig. 1c, d). In *N. benthamiana* plants at 60 days after sowing (DAS), both *NbBPS1* and *NbBPS2* transcripts were detected in all of the tissues examined, including roots, stems, open flowers, flower buds, and leaves (Fig. 1d). In seedlings at 7 DAS, transcript levels of both genes were higher in roots than in shoots (Fig. 1c).

### Subcellular localization of *NbBPS1*

We examined the subcellular localization of the *NbBPS1* protein by expression of *NbBPS1*:GFP, in which full length *NbBPS1* (M1 to K352) was fused to green fluorescent protein (GFP). The DNA construct containing *NbBPS1*:GFP under the control of the CaMV35S promoter was introduced into protoplasts isolated from *N. benthamiana* seedlings. Since it was predicted that *NbBPS1* would be targeted to the endoplasmic reticulum (ER), a BiP:RFP construct encoding a fusion protein between the ER luminal binding protein BiP and red fluorescent protein (RFP) was cotransformed into the protoplasts. After incubation at 25°C for 24 h, gene expression was examined by confocal laser scanning microscopy. The green fluorescent signal of *NbBPS1*:GFP was localized in a reticular membranous network throughout the cytoplasm of the protoplasts, and the signal was overlapped with the BiP:RFP signal, suggesting that *NbBPS1* is mainly targeted to the ER (Fig. 2a). We further demonstrated that the *NbBPS1* localization pattern is similar to that of an ER resident protein bZIP28 (Fig. 2b). GFP:bZIP28 construct in which GFP was fused to the N-terminus of Arabidopsis bZIP28, an ER membrane-associated transcription factor (Liu et al. 2007), was transiently expressed in *N. benthamiana* protoplasts. The protoplasts exhibited green fluorescence in a network-like pattern throughout the cytoplasm similar to that of *NbBPS1*:GFP. As a control, GFP and RFP vectors were cotransformed into *N. benthamiana* protoplasts, and the fluorescence was localized in the cytosol in a diffused pattern (Fig. 2c).

### VIGS phenotypes and suppression of endogenous transcripts

To induce gene silencing of *NbBPS1*, we cloned two different *NbBPS1* cDNA fragments into the TRV-based VIGS

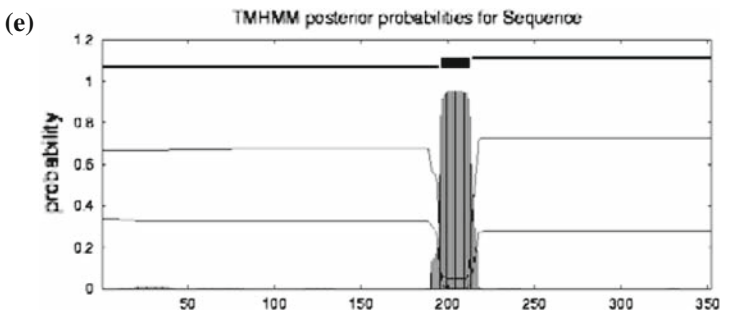
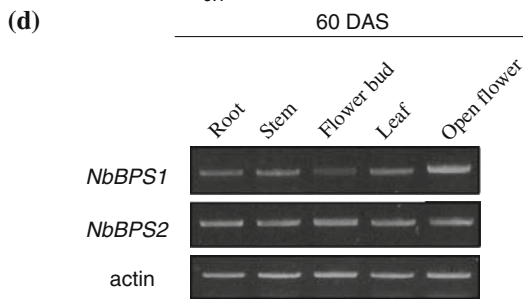
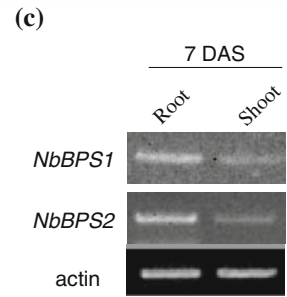
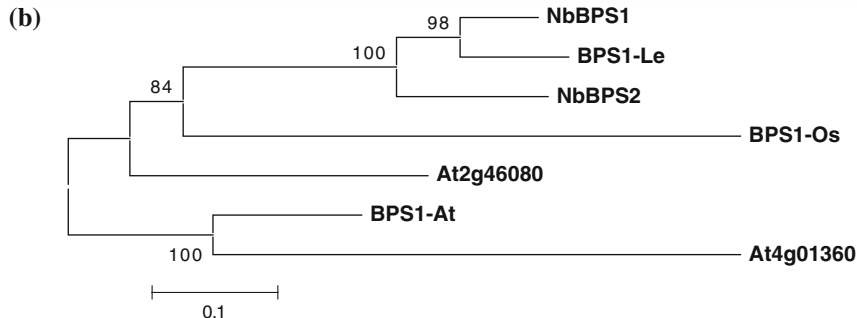
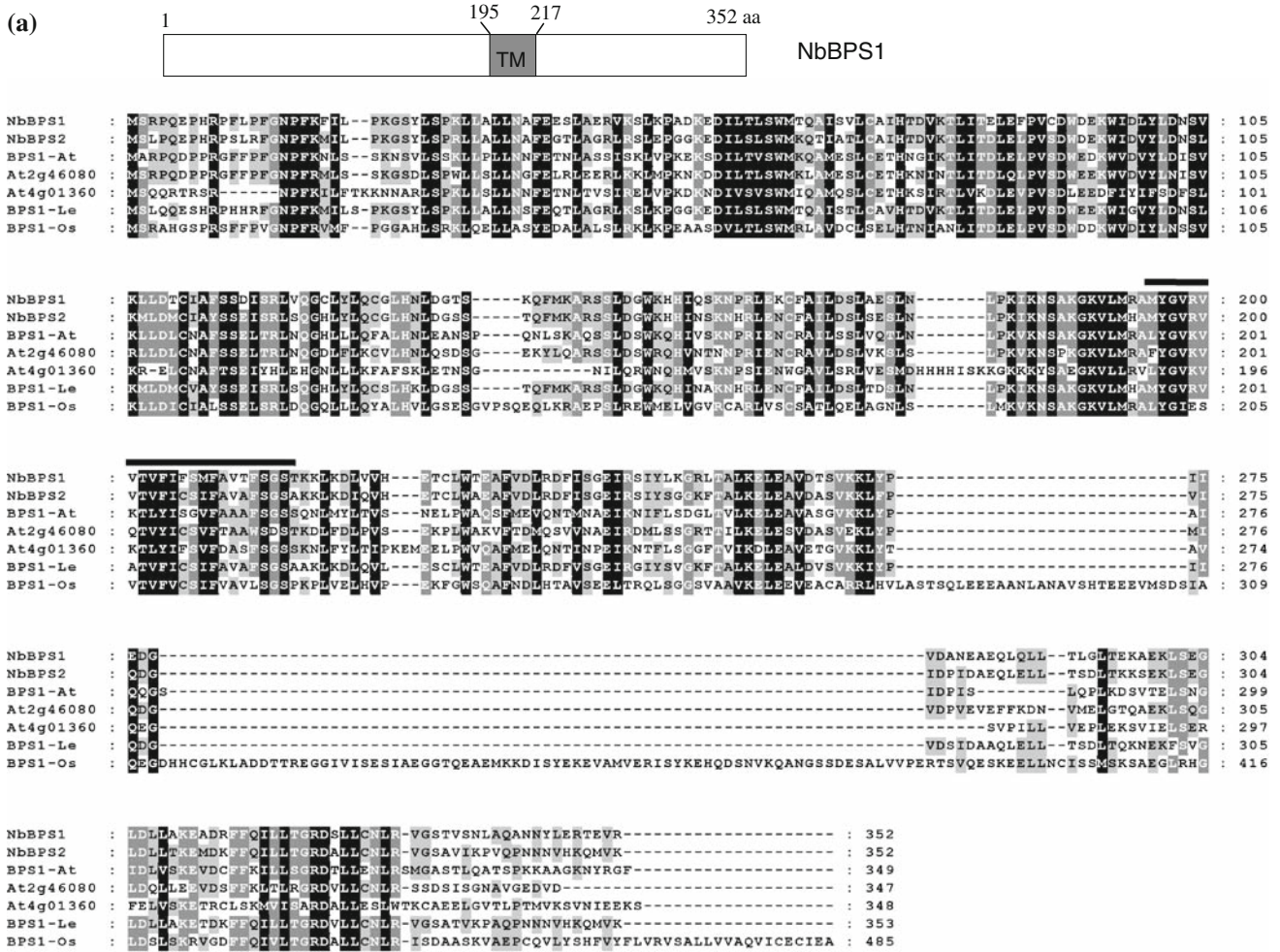


**Fig. 1** Analysis of gene sequences, expression, and protein targeting. (a) Schematic of NbBPS1 protein structure and sequence alignment. The predicted single transmembrane domain (TM) is indicated. Deduced amino acid sequences of *NbBPS1* and *NbBPS2* are aligned with three *Arabidopsis BPS* homologs, *BPS1*, At2g46080, and At4g01360, and related sequences from rice (*BPS1-Os*) and tomato (*BPS1-Le*). The numbers indicate amino acid residues. Residues that are conserved between the sequences are boxed in black or light gray based on the degree of conservation. The transmembrane domain is indicated by the overline. (b) Phylogenetic tree of NbBPS1 and related sequences based on Molecular Evolutionary Genetics Analysis (MEGA) (<http://www.megasoftware.net/>) (Tamura et al. 2007). The tree branches are labeled with the percentage support (only when >50%) for the partition based on 1,000 bootstrap replicates. The scale bar equals a distance of 0.1. (c) Semiquantitative RT-PCR analysis of *NbBPS1* and *NbBPS2* expression in shoots and roots of *N. benthamiana* at 7 days after sowing (DAS). The PCR primers correspond to the 3'-untranslated region of *NbBPS1* and *NbBPS2*. Actin mRNA levels were included as a control. (d) Semiquantitative RT-PCR analysis of *NbBPS1* and *NbBPS2* expression in *N. benthamiana* tissues at 60 DAS using the same PCR primers as for Fig. 1c. (e) A plot for probabilities of a transmembrane domain in the NbBPS1 protein sequence analyzed by TMHMM program (<http://www.cbs.dtu.dk/services/TMHMM/>). >90% probability of a transmembrane domain was predicted for residues 195–217

vector pTV00 (Kim et al. 2006), and infiltrated *N. benthamiana* plants with *Agrobacterium* containing each plasmid (Fig. 3a). TRV:BPS1(U) and TRV:BPS1(C) contained a 278 bp 3'-untranslated (UTR) region and a 605 bp C-terminal region of the *NbBPS1* cDNA, respectively. The TRV:GFP control contained the green fluorescent protein cDNA. VIGS with each of the *BPS1* constructs resulted in growth retardation (Fig. 3b), visible at 10 days after infiltration, followed by the production of clusters of malformed yellowish leaves with abnormal vascular patterning at the shoot apex (Fig. 3b, c). The length and the mass of the root were only mildly affected (Fig. 3d; results not shown). Interestingly, in contrast to the *NbBPS1* 3'-UTR, VIGS with a 104 bp *NbBPS2* 3'-UTR produced no visible VIGS phenotype (Fig. 3g).

The effect of VIGS on endogenous *NbBPS1* mRNA levels was examined by semi-quantitative RT-PCR using leaf RNA (Fig. 3f). RT-PCR using BPS1-C2 primers showed significantly reduced PCR product in the TRV:BPS1(C) and TRV:BPS1(U) lines relative to the TRV:GFP lines, indicating that the endogenous level of *NbBPS1* transcripts is greatly reduced in those plants. PCR with BPS1-UTR primers revealed high levels of viral genomic transcripts containing the 3'-UTR region of *NbBPS1* in both TRV:BPS1(C) and TRV:BPS1(U) lines. These results demonstrate that the aberrant phenotypes observed in these lines correlate with the suppression of *NbBPS1* expression.

We next tested whether VIGS with *NbBPS1* cDNAs caused cross-silencing of *NbBPS2* (Fig. 3f). Using BPS2-UTR primers corresponding to the 3'-UTR of *NbBPS2*, little PCR product was amplified in the BPS1(C) VIGS plants, whereas control levels of PCR products were

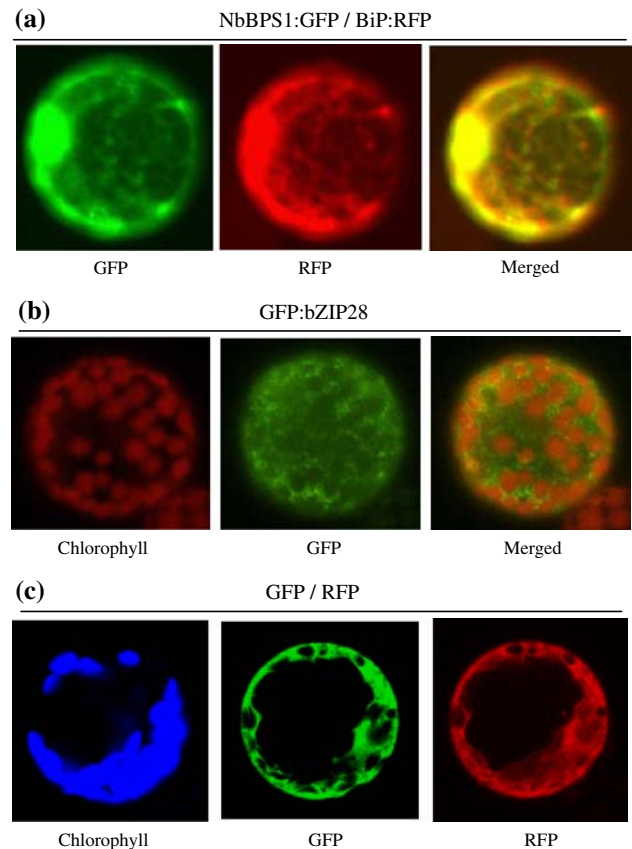


**Fig. 2** Localization of NbBPS1 in the endoplasmic reticulum (ER). (a) The NbBPS1:GFP and the BiP:RFP fusion constructs were cotransformed into *N. benthamiana* protoplasts, and their expression was monitored at 24 h after transformation by fluorescent microscopy. BiP is an ER luminal binding protein. (b) The bZIP28:GFP construct was transformed into *N. benthamiana* protoplasts to show its expression in the ER using fluorescent microscopy. Chloroplasts were visualized by chlorophyll autofluorescence. (c) The control GFP and RFP vectors were cotransformed into *N. benthamiana* protoplasts and the expression was observed by confocal laser scanning microscopy. Chlorophyll autofluorescence was pseudo-colored blue

produced in the BPS1(U) VIGS plants. Therefore *NbBPS2* expression was silenced by the coding region of *NbBPS1*, but not by its 3'-UTR. This result correlates with the degree of sequence homology between the two genes in the coding and the 3'-UTR regions. We also examined whether *NbBPS1* was silenced in the roots of the NbBPS1 lines (Fig. 3d, e). RT-PCR with BPS1-C1 and BPS1-N primers revealed that endogenous *NbBPS1* transcript levels were not reduced in either NbBPS1 VIGS line, while the BPS1-C1 primers amplified viral genomic transcripts containing the C-terminal region in TRV:BPS1(C) lines (Fig. 3e), indicating that the abnormal phenotype observed in these lines was caused by *NbBPS1* silencing in the aerial organs. We next examined whether *NbBPS2* was silenced in the TRV:BPS2(U) lines that lacked visible phenotypes (Fig. 3g, h) using BPS2-C primers corresponding to the

**Fig. 3** VIGS constructs, phenotypes, and suppression of *NbBPS1* transcripts. (a)

Schematic of the *NbBPS1* cDNA structure and two VIGS constructs containing the cDNA fragments (marked by bars).

The box indicates the protein-coding region of *NbBPS1*. The positions of the *BPS1-UTR*, *BPS1-C2*, *BPS1-C1*, and *BPS1-N* primer sets that were used in RT-PCR analyses are also shown. (b) VIGS phenotypes. Photographs of the plants were taken at 30 days after

infiltration (DAI). (c) Leaf morphology at 30 DAI. (d)

Comparison of the root length at 30 DAI. The bars are marked 5 cm apart. (e)

Semiquantitative RT-PCR analysis of endogenous *NbBPS1* mRNA levels in roots using *BPS1-C1* and *BPS2-N* primers. (f)

Semiquantitative RT-PCR analysis of the *NbBPS1* mRNA levels in the leaf using RNA extracted from the fourth leaf above the

infiltrated leaves and *BPS1-UTR*, *BPS1-C2*, and *BPS2-UTR* primer sets. The *BPS2-UTR* primers correspond to the 3'-

UTR of the *NbBPS2* gene. (g) Lack of VIGS phenotypes in the TRV:*BPS2(U)* line containing an 104 bp 3'UTR sequence of

*NbBPS2*. (h) Semiquantitative RT-PCR analysis to examine the specificity of gene silencing. The *BPS1-C2* and *BPS2-C*

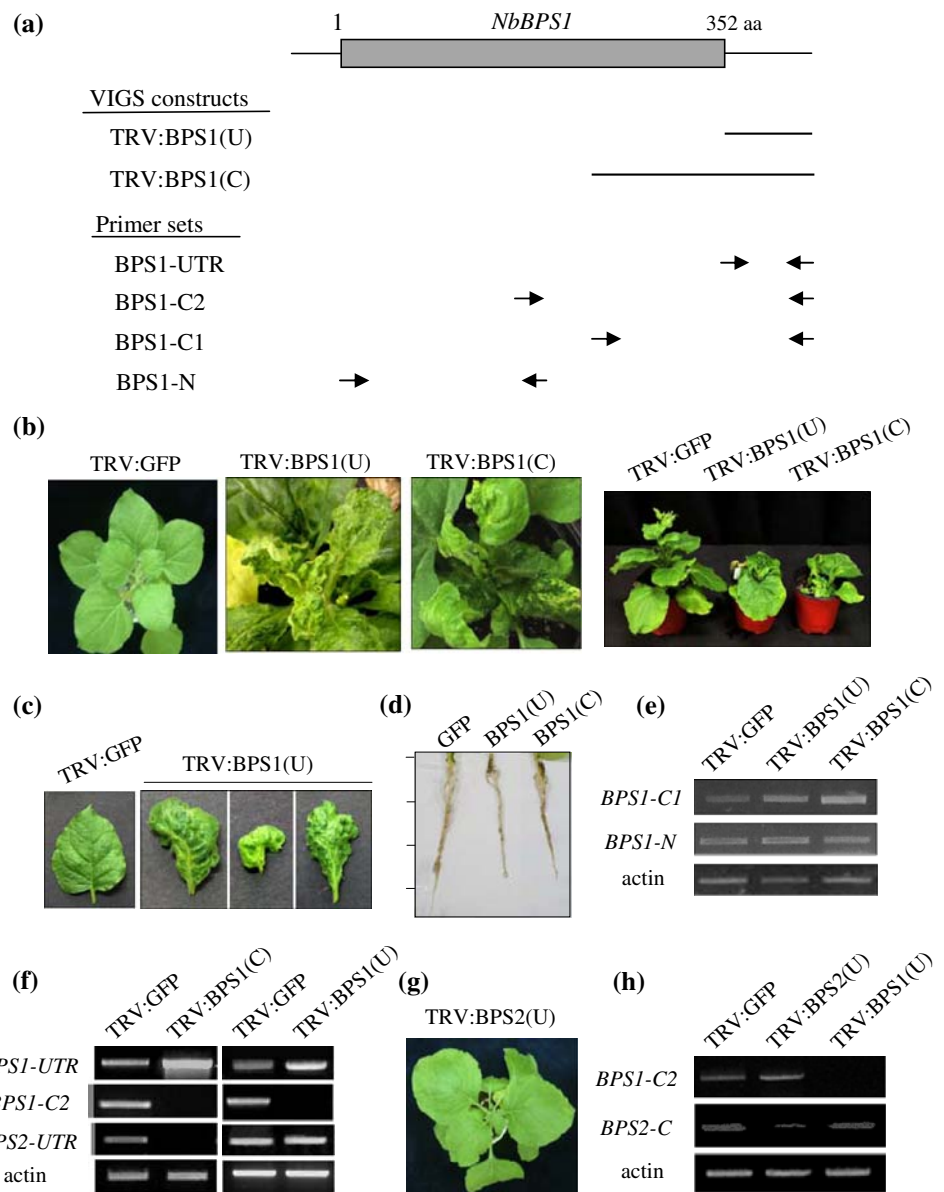
primers were used

coding region (upstream primer) and 3'-UTR (downstream primer) of *NbBPS2*. RT-PCR results suggest that VIGS using the 3'-UTR of *NbBPS1* and *NbBPS2* specifically silenced *NbBPS1* and *NbBPS2* respectively, without cross-silencing each other (Fig. 3h). Since the TRV:*BPS1(C)* lines frequently showed more severe phenotypes than the TRV:*BPS1(U)* lines (Supplementary Fig. 1a), the lack of phenotype in the *BPS2(U)* VIGS line may be caused by incomplete silencing of *NbBPS2* due to the short (104 bp) *NbBPS2* 3'-UTR sequence (Fig. 3h).

Hyperactive cambium in the stem and the petiole

The stem of the TRV:*BPS1* plants appeared to be thicker than that of the control TRV:*GFP* plants. The stem from TRV:*GFP*, TRV:*BPS1(U)*, and TRV:*BPS1(C)* lines was

cross-sectioned freehand where the fourth leaf above the infiltrated leaf was attached, stained, and observed under light and fluorescence microscopy (Fig. 4a–f). All of the VIGS plants exhibited a continuous ring of vascular tissues with the typical bicollateral organization of xylem and phloem. Based on staining patterns with phloroglucinol (Fig. 4a–c) and aniline blue (Fig. 4d–f), a continuous cambium underwent periclinal division leading to radial files of secondary xylem, and phloem fibers were also observed in the TRV:*GFP* control (Fig. 4d). TRV:*GFP* controls exhibited a smooth boundary defining the interface of the cambium and the cell files of the xylem, indicating that cambial cell divisions and differentiation of the precursor cells into the xylem are coordinated (Fig. 4d). Surprisingly, both TRV:*BPS1(U)* (Fig. 4b, e) and TRV:*BPS1(C)* lines (Fig. 4c, f) contained a large non-lignified



cross-sectioned freehand where the fourth leaf above the infiltrated leaf was attached, stained, and observed under light and fluorescence microscopy (Fig. 4a–f). All of the VIGS plants exhibited a continuous ring of vascular tissues with the typical bicollateral organization of xylem and phloem. Based on staining patterns with phloroglucinol (Fig. 4a–c) and aniline blue (Fig. 4d–f), a continuous cambium underwent periclinal division leading to radial files of secondary xylem, and phloem fibers were also observed in the TRV:*GFP* control (Fig. 4d). TRV:*GFP* controls exhibited a smooth boundary defining the interface of the cambium and the cell files of the xylem, indicating that cambial cell divisions and differentiation of the precursor cells into the xylem are coordinated (Fig. 4d). Surprisingly, both TRV:*BPS1(U)* (Fig. 4b, e) and TRV:*BPS1(C)* lines (Fig. 4c, f) contained a large non-lignified

#### Hyperactive cambium in the stem and the petiole

The stem of the TRV:*BPS1* plants appeared to be thicker than that of the control TRV:*GFP* plants. The stem from TRV:*GFP*, TRV:*BPS1(U)*, and TRV:*BPS1(C)* lines was

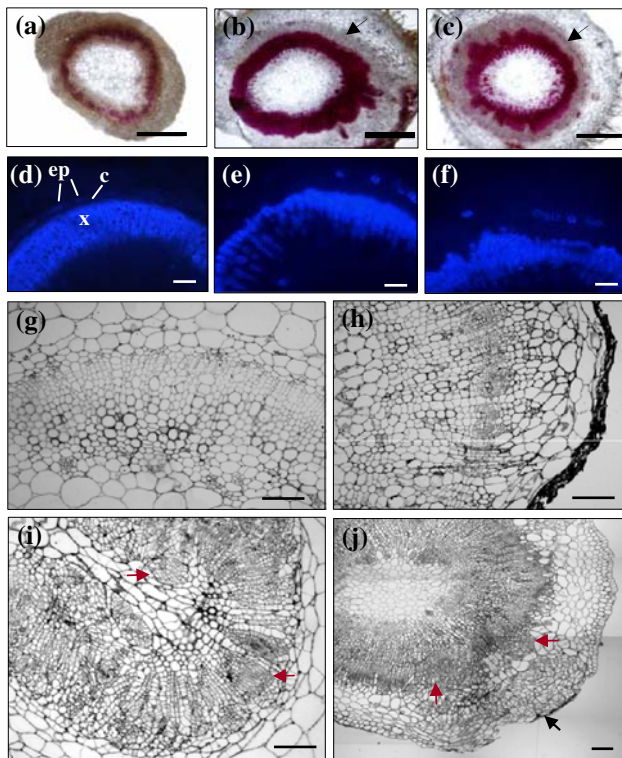


**Fig. 4** Hyperproliferation of the cambial cells. (a–f) Transverse sections of the stem from TRV:GFP (a, d), TRV:BPS1(U) (b, e), and TRV:BPS1(C) (c, f) lines, taken where the fourth leaf above the infiltrated leaf was attached, were stained with phloroglucinol (a–c) and aniline blue (d–f), and observed by light and fluorescence microscopy. The arrows indicate a large non-lignified cell mass in the cambium (b, c). x, xylem; c, cambium; ep, external phloem. Scale bars = 1 mm in (a–c); 200  $\mu$ m in (d–f). (g–j) Thin sections of the stem vascular tissues from TRV:GFP (g), TRV:BPS1(U) (h) and the TRV:BPS1(C) (i, j) lines were observed under light microscopy. The red and black arrows indicate round cell clusters (i, j) and dividing cells in the cortex and the epidermis (j), respectively. Scale bars = 200  $\mu$ m in (g–j)

cell mass in the cambium, resulting in an enlargement of the stele throughout the stem. The boundary of the xylem was erratic with discontinuous xylem cell files in TRV:BPS1(C) lines (Fig. 4f). The abnormal vasculature was also observed at the subapical position of the stem (results not shown). Semiquantitative RT-PCR with BPS1-C2 primers using RNA extracted from the stem of TRV:BPS1(C) and TRV:BPS1(U) lines indicated that the observed stem phenotype is caused by silencing of *NbBPS1* (Supplementary Fig. 1b).

The altered vasculature of TRV:BPS1 stems was examined in detail using thin sections. TRV:BPS1(U) stems exhibited an unusually active cambium with hyperproliferating cells dividing at random direction (Fig. 4h, cf. control in 4 g). In more severe cases, as in TRV:BPS1(C) lines, multiple round cell clusters were formed in the cambium as well as in the pith (Fig. 4i, j; cf. control in 4g).

Furthermore, this uncontrolled proliferating activity was also detected in other cell layers including the cortex and the epidermis (Fig. 4j). The phloem was no longer discernable among the dividing cells, and the pith was substantially shrunken due to the hyperactive cell division in TRV:BPS1 stems (Fig. 4i, j). Similarly, excessive cell division was also observed in the vascular tissues of the petiole in the TRV:BPS1(U) and TRV:BPS1(C) lines (data not shown). Taken together, these results indicate that *NbBPS1* plays a critical role in the control of the cambial activity in the stem and the petiole of *N. benthamiana*.

#### Defective xylem differentiation

The cell mass present in the vascular tissues of the TRV:BPS1 stem was examined further by transmission electron microscopy (Fig. 5). The TRV:GFP control exhibited the typical morphology of phloem, cambium, and xylem in the stem vasculature (Fig. 5a–e). Figure 4e shows a tracheary element (TE) with the secondary wall being formed and the primary wall being degraded and modified. The TRV:BPS1 stems showed highly proliferated but randomly organized cell files (Fig. 5f–o). The majority of the cells in the cell mass from the TRV:BPS1(U) (Fig. 5f–j) and TRV:BPS1(C) stems (Fig. 5k–o) seemed to be xylem cells arrested at various stages of differentiation, since the secondary growth most actively produces xylem in tobacco. Some cells had undergone autolysis, entirely lacking the tonoplast, cytoplasm, and organelles (Fig. 5g–j), while others still had fragmented cytoplasm that was undergoing degeneration after rupture of the vacuole (Fig. 5m–o). Many cells accumulated osmiophilic materials (Fig. 5g–i, l). The initial deposition of the secondary cell wall was observed in some cells (Fig. 5j), but in general the secondary cell-wall thickening in xylem was significantly delayed in the TRV:BPS1 stems (Fig. 5g–j, l–o). These results suggest that *NbBPS1* deficiency stimulated cambial cell proliferation but inhibited its subsequent differentiation in *N. benthamiana* stem.

#### Hyperproliferation of the cambial cells is correlated with increased auxin and cytokinin levels and/or signaling

We next generated transgenic *N. benthamiana* plants carrying *ARR5::GUS* and *DR5::GUS* reporter genes. The *ARR5* promoter is derived from a response regulator gene of the two-component system that is transcriptionally upregulated by cytokinin (D'Agostino et al. 2000). The *DR5* promoter is responsive to auxin due to the presence of highly active synthetic auxin response elements (Ulmasov et al. 1997). *ARR5::GUS* activity was detected in the shoot and root apical meristems, and in vascular tissues of

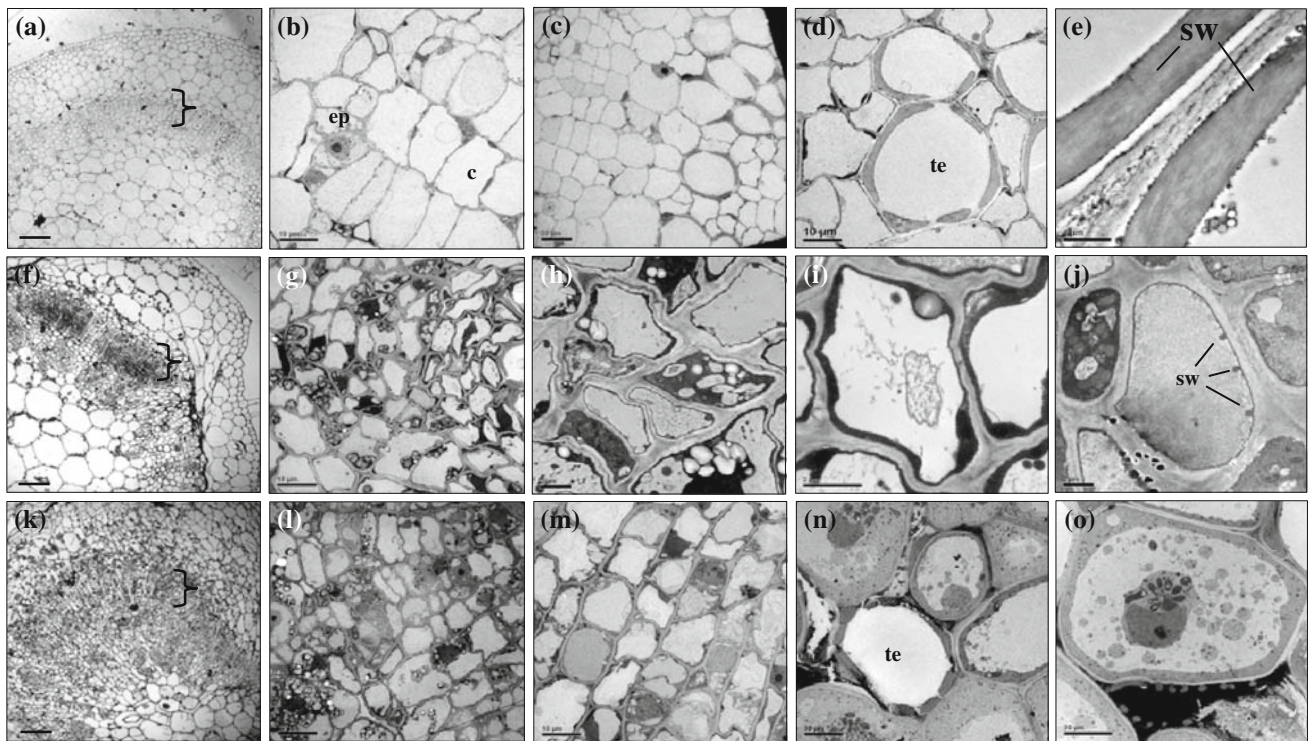


**Fig. 5** Defective xylem differentiation. Thin sections of vascular tissues from the TRV:GFP (a–e), TRV:BPS1(U) (f–j), and TRV:BPS1(C) stems (k–o) were examined using transmission electron microscopy. The brackets indicate the examined area (a, f, k). x,

xylem; c, cambium; ep, external phloem; te, tracheary element; sw, secondary wall. Scale bars = 200  $\mu$ m in (a, f, k); 10  $\mu$ m in (b, d, g, i, m, n, o); 20  $\mu$ m in (c, l); 2  $\mu$ m in (h–j); 1  $\mu$ m in (e)

*N. benthamiana* seedlings at 7 days after germination (Fig. 6a–d), similar to the expression pattern observed in *Arabidopsis* (D’Agostino et al. 2000). *DR5::GUS* activity was detected in the root apical meristems, developing vascular tissues in the cotyledon, and the tip of a young primordium (Fig. 6m–o), also observed in *Arabidopsis* (Aloni et al. 2003). *DR5::GUS* expression was induced by IAA in the vascular tissues of the hypocotyl and the root (Fig. 6p). To investigate whether the uncontrolled cell division in the TRV:BSP1 cambium is associated with increased auxin/cytokinin levels and/or signaling, NbBPS1 VIGS was carried out in *DR5::GUS* and *ARR5::GUS* transgenic backgrounds. At 20 days after infiltration, the fully expanded leaf and the stem of the TRV:GFP control in either a *DR5::GUS* or *ARR5::GUS* background displayed little *GUS* staining (Fig. 6e–g, q; results not shown), whereas TRV:BPS1(C) lines exhibited strong *ARR5::GUS* activity in the vascular tissues of the stem and the petiole (Fig. 6h–l), and strong *DR5::GUS* activity in the vascular tissues of the stem (Fig. 6r–u). Interestingly, *DR5::GUS* expression was detected in the whole vascular bundle in the stem (Fig. 6r–u), while *ARR5::GUS* expression was frequently detected in the outermost boundary of the cambium (Fig. 6j, k) and the cortex (Fig. 6j, l). This increased *DR5::GUS* and *ARR5::GUS* activity may indicate that

abnormally increased auxin/cytokinin levels and/or signaling contribute to the hyperactivity of the cambium. Alternatively, promoter activities of *DR5* and *ARR5* might have been stimulated due to the vascular defects.

#### Cell enlargement and enhanced endoreduplication in the TRV:BPS1 leaf

In contrast to the reduced size of the stem vascular cells due to stimulated cell division, the leaf cell size increased in TRV:BPS1 lines (Fig. 7b, d, f; cf. control in 7a, c, e). Transverse leaf sections revealed that TRV:GFP control leaves had the typical leaf structure of dicotyledonous plants with distinct adaxial and abaxial epidermal layers (Fig. 7a). In the TRV:BPS1(C) lines, the typical dorsoventral organization of the palisade and spongy mesophyll cells was mostly maintained, but the lamina was thicker due to the increased cell size in all layers (Fig. 7b). Scanning electron microscopy of both adaxial and abaxial epidermal layers of the TRV:BPS1(C) lines also showed enlarged cells (Fig. 7d, cf. control in 7c; data not shown) as did light microscopy of the peeled abaxial epidermis (Fig. 7f, cf. control in 7e). The epidermal cell morphology remained normal. The relative area of leaf protoplasts from the TRV:BPS1(C) lines was enlarged  $\sim 2.2$ -fold compared





**Fig. 6** Increased auxin and cytokinin levels and/or response. VIGS was performed using transgenic *N. benthamiana* plants carrying the *ARR5::GUS* or the *DR5::GUS* fusion genes. (a–d) Transgenic *N. benthamiana* plants carrying the *ARR5::GUS* fusion gene exhibited GUS staining in the shoot apex, the root apex, and developing vascular tissues at 7 days after sowing (DAS). (e–g) Control VIGS in the *ARR5::GUS* plants resulted in no visible GUS staining in the leaves and the stems at 20 days after infiltration (DAI). (h–l) BPS1(C) VIGS in the *ARR5::GUS* plants caused strong GUS expression in the vascular tissues of the petiole (h, i) and the stem (j) at 20 DAI.

Specifically, the GUS activity was concentrated in the outer boundary of the cambium (k) and the cortex (l). (m–p) Transgenic *N. benthamiana* plants carrying the *DR5::GUS* fusion gene exhibited GUS staining in the tip of the leaf primordium, the root apex, and developing vascular tissues at 7 DAS (m–o). IAA (1  $\mu$ M) induced GUS expression in the vascular tissues of the seedlings (p). (q) Control VIGS in *DR5::GUS* plants resulted in no visible GUS staining in the stem at 20 DAI. (r–u) BPS1(C) VIGS in *DR5::GUS* plants caused GUS expression in the whole stem vasculature at 20 DAI

with TRV:GFP (Fig. 7g). Considering that the leaf size of the TRV:BPS1(C) lines was similar to or smaller than the control, the enlargement of cell size suggests a reduction in

leaf cell numbers. It has been reported that reduced cell division is frequently compensated for by an increase in cell expansion, and cell enlargement has been used as an

indicator of reduced cell division in plants (Donnelly et al. 1999; De Veylder et al. 2001; Kessler and Sinha 2004). Further study would reveal an underlying mechanism of the growth arrest and cell size increase in the leaf of the TRV:BPS1 plants.

Endoreduplicating cells undergo iterative DNA replication without subsequent mitosis resulting in a higher-ploidy nucleus, a phenomenon associated with cell enlargement in plants (Joubès and Chevalier 2000; Sugimoto-Shirasu and Roberts 2003). Using flow cytometry, we measured and quantified the ploidy levels in nuclei isolated from mature leaves or stems of TRV:GFP and TRV:BPS1 lines (Fig. 7h–k). In TRV:GFP control leaves, almost all nuclei had a ploidy level of 2C, consistent with previous studies in *N. tabacum* and *N. benthamiana* (Kosugi and Ohashi 2003; Park et al. 2005). However, nuclei from the independent TRV:BPS1(U) and TRV:BPS1(C) lines exhibited increased numbers of nuclei with a ploidy level of 4C and some nuclei even reached 8C (Fig. 7h, j). Thus, BPS1 deficiency led to increased ploidy levels in the leaves, which correlated with cell enlargement. In contrast, there was no increase in the level of endoreduplication in the stem cells, which were not enlarged (Fig. 7i, k).

The cell death phenotype in the TRV:BPS1 leaf

The NbBPS1 VIGS plants did not show obvious exterior necrotic lesions, but microscopic examination of the leaves revealed abnormalities in cell structure (Fig. 8). Using confocal laser scanning microscopy, defects in chloroplasts and mitochondria could be observed in leaf protoplasts within 2 weeks after infiltration (Fig. 8a–c). In both TRV:BPS1(C) and TRV:BPS1(U) lines, almost all of the protoplasts exhibited significantly reduced chloroplast numbers (about 26% and 28% of those in the TRV:GFP control, respectively) (Fig. 8a, b). Mitochondria in leaf protoplasts were examined by TMRM staining, which indicates mitochondrial membrane potential (Fig. 8a, c). The TMRM fluorescence of protoplasts from TRV:BPS1(C) and TRV:BPS1(U) leaves was significantly lower than in leaves from the TRV control, suggesting reduced mitochondrial numbers and/or membrane potential. Transmission electron microscopic analysis of the leaf cells from the TRV:BPS1(C) lines showed degenerating organelles and other cellular structures (Fig. 8e–i; cf. control in 8d). The vacuoles were ruptured (Fig. 8e), and numerous vesicle-like structures were formed from the plasma membrane (Fig. 8h, i).

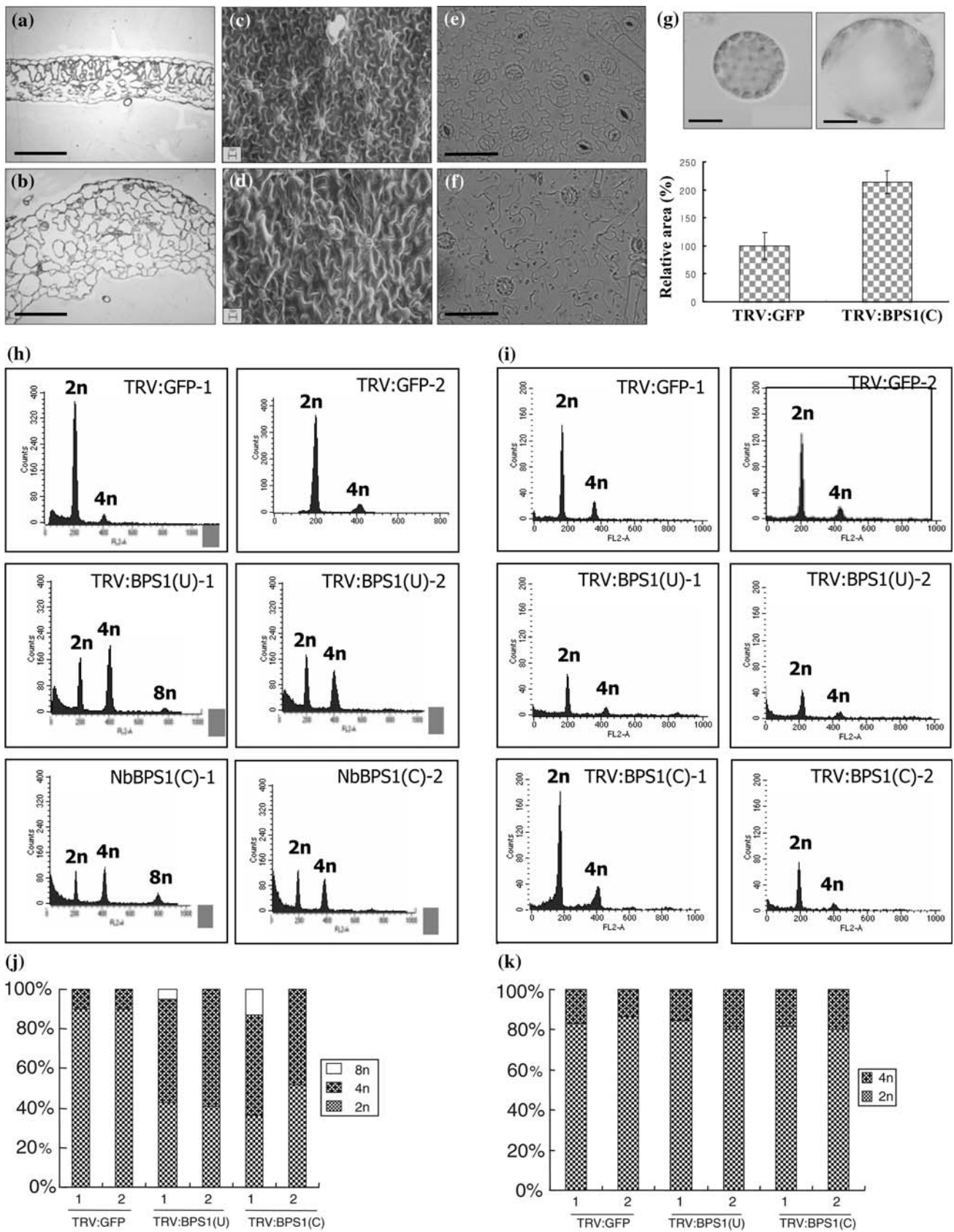
## Discussion

The *Arabidopsis bypass1* (*bps1*) mutant exhibits defective growth and abnormal leaf and root development (Van

**Fig. 7** Cell enlargement and increased endoreduplication. The fourth leaf above the infiltrated leaf from the VIGS lines was used. (a–b) Light micrographs of transverse sections through the central part of the leaf from TRV:GFP (a) and TRV:BPS1(C) (b) lines. Scale bars = 100  $\mu$ m. (c–d) Scanning electron micrographs of the abaxial epidermis from TRV:GFP (c) and TRV:BPS1(C) (d) lines. Scale bars = 20  $\mu$ m. (e–f) Light micrographs of the abaxial epidermis of TRV:GFP (e) and TRV:BPS1(C) (f) lines. Scale bars = 100  $\mu$ m. (g) Representative leaf mesophyll protoplasts from TRV:GFP (top, left) and TRV:BPS1(C) lines (top, right). Scale bars = 20  $\mu$ m. The size of 90–100 protoplasts was analyzed by light micrography and displayed as bar graphs (bottom). (h) Ploidy distribution of leaf nuclei from representative TRV:GFP and TRV:BPS1(C) lines. Nuclei were stained with propidium iodide and analyzed by flow cytometry. (i) Ploidy distribution of the stem nuclei from representative TRV:GFP and the TRV:BPS1(C) lines. (j) Quantification of the ploidy levels in (h). (k) Quantification of the ploidy levels in (i)

Norman et al. 2004). Based on grafting experiments, it has been proposed that BPS1 function is required to inhibit production of root-derived carotenoid-related signaling molecules that are capable of arresting shoot growth (Van Norman et al. 2004). Production of this signal has been shown to require synthesis of  $\beta$ -carotene and its derivatives, but the identity of the signal is unknown (Van Norman and Sieburth 2007). During VIGS analysis in *N. benthamiana*, we found that silencing of *NbBPS1* induced severe growth defects, and further investigated how NbBPS1 deficiency affects different target tissues.

Although many vascular mutants have been identified in plants, only a few demonstrate increased cambial activity. The *Arabidopsis high cambial activity* (*hca*) mutation results in a continuous ring of xylem and phloem in the stem as a consequence of increased cambial cell division in both the fascicular and interfascicular regions (Pineau et al. 2005). Moreover, *hca* mutants exhibit an altered auxin and cytokinin response, in particular an enhanced sensitivity to cytokinin, indicating that *HCA* is involved in the control of vascular organization by regulating the auxin-cytokinin sensitivity of vascular cambium. The *HCA* gene has not been cloned (Pineau et al. 2005). The *continuous vascular ring1* (*cov1*) mutation significantly increases vascular tissue development in the stem at the interfascicular region (Parker et al. 2003). The *Arabidopsis cov1* mutant displays normal vascular patterns in other organs and auxin sensitivity was not affected. The *COV1* gene encodes a membrane protein of unknown function, although *COV1* is thought to be involved in an auxin-independent mechanism that negatively regulates the differentiation of vascular tissues in the stem (Parker et al. 2003). Ectopic expression of *ATHB-8*, which encodes a member of the homeodomain-leucine zipper (HD-Zip) III family of transcription factors, in *Arabidopsis* increases xylem production caused by stimulated vascular cell differentiation (Baima et al. 2001; Jung and Park 2007). The procambial cells differentiate



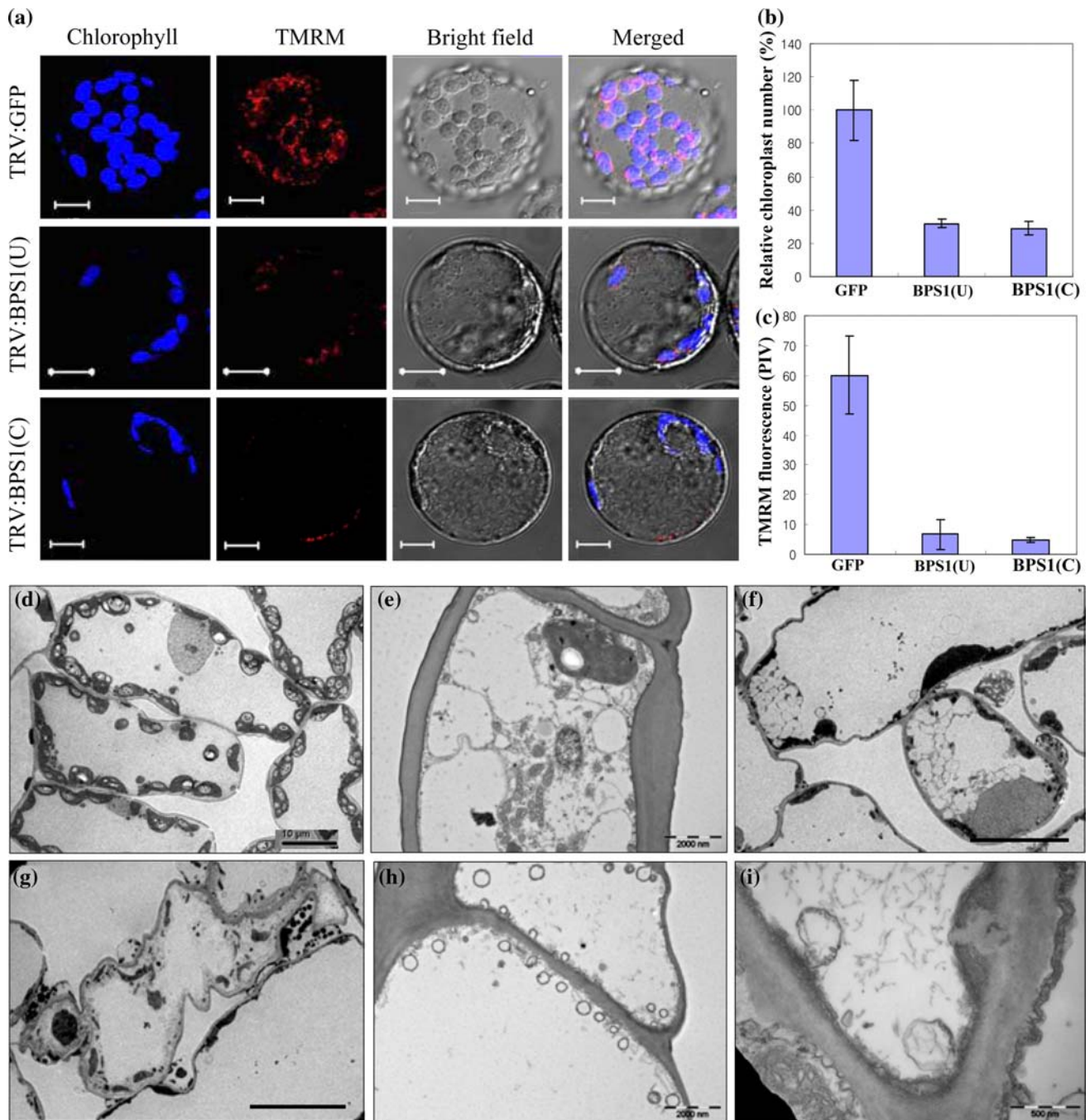


**Fig. 8** Cell death phenotypes in the leaf. **(a)** Confocal laser scanning microscopy of chloroplasts and mitochondria at 14 DAI. To visualize mitochondria, leaf protoplasts were stained with 200 nM TMRM. Scale bars = 10  $\mu$ m. **(b)** The average number of chloroplasts per protoplast in the TRV:GFP control was 56. Data points represent means  $\pm$  SD of thirty individual protoplasts, expressed as a

percentage of the TRV:GFP control. **(c)** Mitochondrial membrane integrity was measured by TMRM staining. Data points represent means  $\pm$  SD of thirty individual protoplasts. PIV, pixel intensity values. **(d-i)** Transmission electron micrographs of leaf mesophyll cells from TRV:GFP **(d)** and TRV:BPS1(C) **(e-i)** lines. Scale bars = 10  $\mu$ m in **(d, f, g)**; 2  $\mu$ m in **(e, h)**; 0.5  $\mu$ m in **(i)**

precociously into primary xylem, and the transition to secondary growth occurs prematurely in the stems of the transgenic plants, indicating that *ATHB-8* is a positive regulator of proliferation and differentiation of procambial and cambial cells (Baima et al. 2001). Compared with the

vascular mutants and the *ATHB-8* overexpressing plants described above, the NbBPS1 VIGS plants exhibited a more dramatic increase in cambial activity, leading to production of a large mass of xylem cells, which appeared to be arrested at various stages of differentiation. This

phenotype does not mimic any of the vascular mutant phenotypes identified to date and may suggest a novel mechanism of action for NbBPS1 in the control of vascular development.

Hyperproliferation of the cambial cells in NbBPS1 VIGS lines was correlated with increased auxin-cytokinin levels and/or signaling (Fig. 6). Auxin plays a critical role in the control of cambial activity and development of primary and secondary vascular tissues by regulating both radial and longitudinal vascular patterning (Ye 2002; Fukuda 2004; Scarpella and Meijer 2004). Auxin efflux carrier PIN1, involved in polar auxin transport, and PINOID and MONOPTEROS, involved in auxin response, are all required for vascular development (Gälweiler et al. 1998; Hardtke and Berleth 1998; Christensen et al. 2000). Cytokinin also appears to be involved in vascular differentiation (Ye 2002). The Arabidopsis *wooden leg* (*wol*) mutation resulted in a reduced number of procambial cells in the embryo and exclusive xylem differentiation in the vascular tissue (Mähönen et al. 2000, 2006). *WOL/CRE1* encodes a histidine kinase that functions as a cytokinin receptor, and is preferentially expressed in the procambium. These observations suggest that cytokinin regulates vascular development by controlling procambial cell division. Furthermore, during xylogenesis of *Zinnia elegans* cultures, differentiation from the dedifferentiated cells to procambium-like cells requires both auxin and cytokinin (Fukuda and Komamine 1980). In this study, NbBPS1 deficiency led to an enhanced auxin/cytokinin response in the cambium, which subsequently resulted in the activation of extensive cambial cell division. The mechanism underlying the altered hormonal response caused by *NbBPS1* down-regulation is not known. Surprisingly, cell proliferation was occasionally stimulated in nonmeristematic tissues including the cortex, the pith, and the epidermis of the stem (Fig. 4), accompanied by increased *ARR5* promoter activity in these tissues (Fig. 6). Cytokinin is not only essential for progression through the cell cycle, but also plays a role in releasing cells that are arrested at the G0 state (den Boer and Murray 2000; Francis 2007). It is possible that enhanced cytokinin level and/or sensitivity in the nonmeristematic tissues induce cell cycle entry in NbBPS1 VIGS lines.

Differentiation of the overproduced xylem cells was defective in the NbBPS1 VIGS lines (Fig. 5). The differentiation process of tracheary elements (TEs) involves two main events: secondary wall formation and programmed cell death (PCD) (Fukuda 2004; Nieminen et al. 2004). A critical step in TE PCD is the transcriptional activation of PCD-specific genes including various hydrolytic enzymes that are transported to the vacuole for activation. The cell death program in TEs is tightly coupled with secondary wall deposition, and to date no mutation has separately affected

these two processes, indicating that these two programs are molecularly interdependent (Fukuda 2004). In *Z. elegans* cell cultures, approximately 6 h after secondary wall thickenings become visible the central vacuole rapidly collapses leading to enzymatic degradation of cell contents including nuclear and chloroplast DNA (Groover and Jones 1999; Obara et al. 2001). However, in the NbBPS1 VIGS lines, the majority of the overproduced xylem cells appeared to undergo autolysis without secondary wall thickening (Fig. 5). Some cells exhibited numerous cytosolic fragments, possibly in the process of vacuole collapse or in a stage soon thereafter, while other cells appeared to be cleared of any recognizable structures and contained only the osmiophilic remains. Secondary wall synthesis was not evident in either situation. Thus, NbBPS1 deficiency appeared to disrupt the coordination of secondary wall thickening and PCD during TE differentiation, resulting in premature vacuolar rupturing and release of the hydrolytic enzymes. Furthermore, the finding that many cells were in the middle of the degeneration process indicates that the PCD process itself did not progress normally, since TE autolysis has been shown to be rapid (Groover and Jones 1999; Obara et al. 2001).

VIGS of *NbBPS1* resulted in growth arrest of *N. benthamiana*. The growth arrest in the NbBPS1 VIGS lines is likely caused by the abnormal stem vasculature. According to previous reports, lack of Arabidopsis BPS1 function may lead to production of novel root-derived carotenoid-related signaling molecules that inhibit shoot growth (Van Norman et al. 2004; Van Norman and Sieburth 2007). However, it has been shown that VIGS does not work efficiently in the root due to the inefficient invasion of root systems by viruses including TRV (Valentine et al. 2004). Furthermore, Fig. 3e showed that *NbBPS1* was not silenced in the root of the NbBPS1 VIGS lines. Thus, the NbBPS1 VIGS phenotypes such as growth arrest and cambium hyperproliferation are presumably caused by silencing of the gene in the aerial parts of the plant. *NbBPS1* and *NbBPS2* transcripts were consistently detected in all *N. benthamiana* tissues tested (Fig. 1d). The phenotypic effects by *NbBPS1* down-regulation in the aerial organs indicate that mechanism of NbBPS1 function is somewhat different from that of Arabidopsis BPS1.

NbBPS1:GFP fusion protein was mainly localized in the ER (Fig. 2). The NbBPS1 protein has a central transmembrane domain (M195 to A217) based on TMHMM (<http://www.cbs.dtu.dk/services/TMHMM/>) and PSORT (<http://psort.hgc.jp/>) programs (Fig. 1e), and it was predicted that the N-terminal half would be exposed to the cytosol (<http://psort.hgc.jp/>). Supplementation with fluridone, an inhibitor of the carotenoid biosynthetic enzyme phytoene desaturase, partially rescued the NbBPS1 VIGS phenotype (Supplementary Fig. 2), indicating that *NbBPS1*

deficiency in the aerial organs also leads to accumulation of the carotenoid-related signal. The production of the mobile carotenoid-derived signal requires cleavage of carotenoid precursors, mainly catalyzed by carotenoid cleavage dioxygenases (CCDs). Although many of the CCD enzymes are localized in the plastid, some of the enzymes are located in the cytosol or attached to the outer envelope of the plastid (Bouvier et al. 2003; Simkin et al. 2004). ER-localized NbBPS1 may interact with carotenoid cleavage enzymes localized in the cytosol or attached to the plastid outer envelope, and regulate their activities. While the molecular nature of the carotenoid-related signal remains unknown, in this study we have shown that the signaling molecules differentially affect cell proliferation activity in the cambium and the shoot apex, possibly by modulating auxin/cytokinin levels and/or response. Interestingly, the MAX-dependent apocarotenoid hormone controls shoot branching by regulating auxin transport (Bennett et al. 2006). Identification of the mobile carotenoid-derived signal, and characterization of the biochemical function of BPS1 proteins and their interaction with hormone signaling pathways would give further insight into the mechanism by which BPS1 regulates development of plant organs.

**Acknowledgements** The authors wish to thank Dr. Tom J. Guilfoyle (University of Missouri, USA) for providing the *DR::GUS* construct, and Drs. Jeong Ho Roh and Hye Kyung Rhee (National Horticultural Research Institute, Korea) for providing a technical help for flow cytometry. This research was supported by grants from the Plant Diversity Research Center of the 21st Century Frontier Research Program, a KOSEF grant (M10749000002-07N4900-00210), and the Plant Signaling Network Research Center (at Korea University) of the Science Research Center Program, all of which are funded by the Ministry of Science and Technology of Korea.

## References

- Ahn J-W, Kim M, Lim JH, Kim G-T, Pai H-S (2004) Phytoalexin controls the proliferation and differentiation fates of cells in plant organ development. *Plant J* 38:969–981
- Aloni R, Schwalm K, Langhans M, Ullrich CI (2003) Gradual shifts in sites of free-auxin production during leaf-primordium development and their role in vascular differentiation and leaf morphogenesis in *Arabidopsis*. *Planta* 216:841–853
- Baima S, Possenti M, Matteucci A, Wisman E, Altamura MM, Ruberti I, Morelli G (2001) The *Arabidopsis* ATHB-8 HD-zip protein acts as a differentiation-promoting transcription factor of the vascular meristems. *Plant Physiol* 126:643–655
- Bennett T, Sieberer T, Willett B, Booker J, Luschign C, Leyser O (2006) The *Arabidopsis* MAX pathway controls shoot branching by regulating auxin transport. *Curr Biol* 16:553–563
- Booker J, Auldridge M, Wills S, McCarty D, Klee H, Leyser O (2004) MAX3/CCD7 is a carotenoid cleavage dioxygenase required for the synthesis of a novel plant signaling molecule. *Curr Biol* 14:1232–1238
- Bouvier F, Suire C, Mutterer J, Camara B (2003) Oxidative remodeling of chromoplast carotenoids: identification of the carotenoid dioxygenase CsCCD and CsZCD genes involved in *Crocus* secondary metabolite biogenesis. *Plant Cell* 15:47–62
- Cho HS, Lee SS, Kim KD, Kim SJ, Hwang I, Lim JS, Park YI, Pai H-S (2004) DNA gyrase is involved in chloroplast nucleoid partitioning. *Plant Cell* 16:2665–2682
- Cho M, Lee OR, Ganguly A, Cho HT (2007) Auxin-signaling: short and long. *J Plant Biol* 50:79–89
- Christensen SK, Dagenais N, Chory J, Weigel D (2000) Regulation of auxin response by the protein kinase PINOID. *Cell* 100:469–478
- D'Agostino IB, Deruere J, Kieber JJ (2000) Characterization of the response of the *Arabidopsis* response regulator gene family to cytokinin. *Plant Physiol* 124:1706–1717
- De Veylder L, Beeckman T, Beemster GT, Krols L, Terras F, Landrieu I, van der Schueren E, Maes S, Naudts M, Inzé D (2001) Functional analysis of cyclin-dependent kinase inhibitors of *Arabidopsis*. *Plant Cell* 13:1653–1668
- den Boer BG, Murray JA (2000) Triggering the cell cycle in plants. *Trends Cell Biol* 10:245–250
- Dewitte W, Murray JA (2003) The plant cell cycle. *Annu Rev Plant Biol* 54:235–264
- Donnelly PM, Bonetta D, Tsukaya H, Dengler RE, Dengler NG (1999) Cell cycling and cell enlargement in developing leaves of *Arabidopsis*. *Dev Biol* 215:407–419
- Foo E, Turnbull CG, Beveridge CA (2001) Long-distance signaling and the control of branching in the *rms1* mutant of pea. *Plant Physiol* 126:203–209
- Francis D (2007) The plant cell cycle – 15 years on. *New Phytol* 174:261–278
- Fukuda H (2004) Signals that control plant vascular cell differentiation. *Nat Rev Mol Cell Biol* 5:379–391
- Fukuda H, Komamine A (1980) Direct evidence for cytodifferentiation to tracheary elements without intervening mitosis in a culture of single cells isolated from the mesophyll of *Zinnia elegans*. *Plant Physiol* 65:61–64
- Gälweiler L, Guan C, Müller A, Wisman E, Mendgen K, Yephremov A, Palme K (1998) Regulation of polar auxin transport by AtPIN1 in *Arabidopsis* vascular tissue. *Science* 282:2226–2230
- Gegas VC, Doonan JH (2006) Expression of cell cycle genes in shoot apical meristems. *Plant Mol Biol* 60:947–961
- Groover A, Jones AM (1999) Tracheary element differentiation uses a novel mechanism coordinating programmed cell death and secondary cell wall synthesis. *Plant Physiol* 119:375–384
- Gutierrez C (2005) Coupling cell proliferation and development in plants. *Nat Cell Biol* 7:535–541
- Hardtke CS, Berleth T (1998) The *Arabidopsis* gene MONOPTEROS encodes a transcription factor mediating embryo axis formation and vascular development. *EMBO J* 17:1405–1411
- Joubès J, Chevalier C (2000) Endoreduplication in higher plants. *Plant Mol Biol* 43:735–745
- Jung JH, Park CM (2007) Vascular development in plants: specification of xylem and phloem tissues. *J Plant Biol* 50:301–305
- Kessler S, Sinha N (2004) Shaping up: the genetic control of leaf shape. *Curr Opin Plant Biol* 7:65–72
- Kim M, Lim J-H, Ahn CS, Park K, Kim GT, Kim WT, Pai H-S (2006) Mitochondria-associated hexokinases play a role in the control of programmed cell death in *Nicotiana benthamiana*. *Plant Cell* 18:2341–2355
- Kosugi S, Ohashi Y (2003) Constitutive E2F expression in tobacco plants exhibits altered cell cycle control and morphological change in a cell type-specific manner. *Plant Physiol* 132:2012–2022
- Lee YJ, Kim DH, Kim Y-W, Hwang I (2001) Identification of a signal that distinguishes between the chloroplast outer envelope membrane and the endomembrane system *in vivo*. *Plant Cell* 13:2175–2190

- Liu JX, Srivastava R, Che P, Howell SH (2007) An endoplasmic reticulum stress response in Arabidopsis is mediated by proteolytic processing and nuclear relocation of a membrane-associated transcription factor, bZIP28. *Plant Cell* 19:4111–4119
- Mähönen AP, Bonke M, Kauppinen L, Riikonen M, Benfey PN, Helariutta Y (2000) A novel two-component hybrid molecule regulates vascular morphogenesis of the Arabidopsis root. *Genes Dev* 14:2938–2943
- Mähönen AP, Bishopp A, Higuchi M, Nieminen KM, Kinoshita K, Tormakangas K, Ikeda Y, Oka A, Kakimoto T, Helariutta Y (2006) Cytokinin signaling and its inhibitor AHP6 regulate cell fate during vascular development. *Science* 311:94–98
- Nieminen KM, Kauppinen L, Helariutta Y (2004) A weed for wood? Arabidopsis as a genetic model for xylem development. *Plant Physiol* 135:653–659
- Obara K, Kuriyama H, Fukuda H (2001) Direct evidence of active and rapid nuclear degradation triggered by vacuole rupture during programmed cell death in *Zinnia*. *Plant Physiology* 125:615–626
- Park J-A, Ahn J-W, Kim Y-K, Kim SJ, Kim J-K, Kim WT, Pai H-S (2005) Retinoblastoma protein regulates cell proliferation, differentiation, and endoreduplication in plants. *Plant J* 42:153–163
- Parker G, Schofield R, Sundberg B, Turner S (2003) Isolation of COV1, a gene involved in the regulation of vascular patterning in the stem of Arabidopsis. *Development* 130:2139–2148
- Pineau C, Freydier A, Ranocha P, Jauneau A, Turner S, Lemonnier G, Renou JP, Tarkowski P, Sandberg G, Jouanin L, Sundberg B, Boudet AM, Goffner D, Pichon M (2005) hca: An Arabidopsis mutant exhibiting unusual cambial activity and altered vascular patterning. *Plant J* 44:271–289
- Ramirez-Parra E, Desvoyes B, Gutierrez C (2005) Balance between cell division and differentiation during plant development. *Int J Dev Biol* 49:467–477
- Ratcliff F, Martin-Hernandez AM, Baulcombe DC (2001) Tobacco rattle virus as a vector for analysis of gene function by silencing. *Plant J* 25:237–245
- Scarpella E, Meijer AH (2004) Pattern formation in the vascular system of monocot and dicot plant species. *New Phytol* 164:209–242
- Simkin AJ, Schwartz SH, Auldridge M, Taylor MG, Klee HJ (2004) The tomato carotenoid cleavage dioxygenase 1 genes contribute to the formation of the flavor volatiles beta-ionone, pseudoionone, and geranylacetone. *Plant J* 40:882–892
- Sorefan K, Booker J, Haurogné K, Goussot M, Bainbridge K, Foo E, Chatfield S, Ward S, Beveridge C, Rameau C, Leyser O (2003) MAX4 and RMS1 are orthologous dioxygenase-like genes that regulate shoot branching in Arabidopsis and pea. *Genes Dev* 17:1469–1474
- Stirnberg P, van de Sande K, Leyser HMO (2002) MAX1 and MAX2 control shoot lateral branching in Arabidopsis. *Development* 129:1131–1141
- Sugimoto-Shirasu K, Roberts K (2003) “Big it up”: endoreduplication and cell-size control in plants. *Curr Opin Plant Biol* 6:544–553
- Tamura K, Dudley J, Nei M, Kumar S (2007) MEGA4: Molecular Evolutionary Genetics Analysis (MEGA) software version 4.0. *Mol Biol Evol* 24:1596–1599
- Ulmasov T, Murfett J, Hagen G, Guilfoyle TJ (1997) Aux/IAA proteins repress expression of reporter genes containing natural and highly active synthetic auxin response elements. *Plant Cell* 9:1963–1971
- Valentine T, Shaw J, Blok VC, Phillips MS, Oparka KJ, Lacomme C (2004) Efficient virus-induced gene silencing in roots using a modified tobacco rattle virus vector. *Plant Physiol* 136:3999–4009
- Van Norman JM, Sieburth LE (2007) Dissecting the biosynthetic pathway for the bypass1 root-derived signal. *Plant J* 49:619–628
- Van Norman JM, Frederick RL, Sieburth LE (2004) BYPASS1 negatively regulates a root-derived signal that controls plant architecture. *Curr Biol* 14:1739–1746
- Ye ZH (2002) Vascular tissue differentiation and pattern formation in plants. *Annu Rev Plant Biol* 53:183–202